(NASA-CR-184988) MEASUREMENT AND MODELLING OF FLOW AND HEAT TRANSFER IN 180 DEGREE BENDS (Manchester Univ.) 36 p

N90-70148

Unclas

00/34 0239517

Nomenclature

D_H	Hydraulic diameter of duct
k	Turbulence energy
Nu	Nusselt number
P	Pressure
Q	Rate of heating
r	Radial co-ordinate
R_{INNER}, R_{OUTER}	Inner and outer radii of duct passage
Re	Reynolds number based on hydraulic diameter and bulk mean velocity
T	Temperature
T_B	Bulk temperature
T_w	Local wall temperature
U	Mean x-directed velocity
v	Turbulent radial velocity (rms)
V	Secondary (radial) component of velocity
w	Turbulent streamwise velocity (rms)
W	Mean streamwise velocity
W_b	Bulk streamwise mean velocity
x	Cartesian co-ordinate normal to plane of symmetry with origin at lower wall
X	Normalized x co-ordinate X = 0 coincides with lower wall X = 1 coincides with symmetry plane
y	Radial Cartesian co-ordinate with origin at duct centre
Y	Normalized y co-ordinate Y = 1 inside of bend Y = -1 outside of bend
Z	Streamwise co-ordinate (distance or angle around bend)
ε	Turbulence energy dissipation rate

Introduction

The report documents briefly our research explorations on turbulent flow in square sectioned bends aimed at clarifying the nature of the resultant three-dimensional shear flow that develops.

The motivation for the present work has sprung from our earlier computational and experimental studies of flow in a 180° bend with fully-developed (or nearly fully-developed) flow at entry to the bend. The LDA measurements of Chang, Humphrey and Modavi [1] revealed an extremely complex flow structure at 90° around the bend with a secondary maximum in streamwise velocity near the inside of the bend, Figure 1 . Three-dimensional turbulent flow simulations of this flow by Humphrey's team (Chang [2], Chang et al [3]) and repeat calculations at UMIST (Johnson [4]) failed to capture this flow feature, Figure 1 . At the time it was unclear whether this poor agreement arose from:

- the use of an isotropic turbulent viscosity (the standard k-ε eddy-viscosity model);
- the use of "wall functions" to bridge the near-wall layer where viscous effects are important (and where the flow is most strongly three-dimensional);
- some other weakness in the turbulence model, e.g. the equation for ε that determines the effective turbulent length scale through the flow;
- an insufficiently fine mesh.

In subsequent studies Choi (Launder et al [5]) explored all except the first of these possible sources. Briefly, he found that:

- grid refinements in the initial stages of the bend accompanied by a replacement of wall functions by a

fine near-wall mesh and a low-Reynolds-number turbulence model produced substantial improvements at a position 45° into the bend;

- by 90°, however, the improvements were only minor, Figure 1 ;

- adjustments to the ε equation produced major changes in the computed velocity profile - in which secondary peaks were present - yet without achieving any better overall agreement between computation and measurement.

In the overall Berkeley-UMIST research programme for NASA Lewis two lines of exploration have been followed. Firstly, we have sought to replace the eddy-viscosity model by a higher order turbulent closure - an approach which has led to very successful predictions of flow in a circular sectioned bend (Iacovides and Launder [6]). The initial work in this direction was undertaken at Berkeley while computations completed at UMIST are reported hereunder. The second line of research has sprung from the feeling that while fully-developed entry conditions evidently lead to a very challenging flow, they were not ones most representative of gas turbine flows. Accordingly, our attention has turned to documenting the development of a flow through the same 180° duct as used in our convective heat transfer studies (Johnson [4], Johnson and Launder [7]) but with thinner boundary layers at entry to the bend. Although our earlier study had confined attention almost entirely to thermal measurements (since our Berkeley colleagues had already documented the flow field in an identically proportioned apparatus), we have here provided extensive hot-wire data of the mean and rms velocity field at five stations around the bend.

In the time available under the present grant it has not proved possible to undertake predictions of the flow field arising in the above experiment. However, earlier data by Taylor, Whitelaw and Yianneskis [8] of flow around a 90° bend of similar radius ratio and with thin inlet boundary layers have formed the subject of a computational study by Kreskovsky et al

[9]. These predictions employed a simple one-equation eddy-viscosity model and it therefore seemed desirable to ascertain whether a multi-equation approach would achieve closer agreement with the experiments than that reported by Kreskovsky et al.

Section 2 below reports the experimental programme and this is followed in Section 3 by details of the computational study. Finally, Section 4 summarizes the research findings and recommends further computations that they suggest.

2. The Experimental Programme

2.1 Apparatus and Instrumentation

The apparatus for the present study, Figure 2, is that described in Johnson and Launder [7] save that the inlet tangent duct is shortened to six hydraulic diameters and this is preceded by an inlet contraction of 5:1 area ratio. The square sectioned perspex duct has a hydraulic diameter of 90mm (3.5in) and a mean bend radius of 0.61m (23.6in) giving a curvature ratio of 6.75:1.

The boundary layers were tripped approximately one duct diameter downstream of the contraction which led to a boundary layer thickness of about 10mm at the start of the bend for a Reynolds number of 5.8×10^4 based on a bulk fluid velocity determined by passing the air flow through an orifice plate prior to entry to the fan.

Velocity profile traverses were made at three hydraulic diameters upstream of the bend and at the start of the bend using DISA 55P11 and 55P62 single and cross-wire probes. In the bend itself hot-wire measurements were made at stations 45° apart by traversing vertically (the plane of symmetry of the bend being horizontal) a TSI cross-wire probe through access holes in the top plate of the bend. All the velocity field data were taken with the bend unheated.

The subsequent thermal tests employed sheets of Intrex (a

gold film vacuum deposited on a thin, transparent plastic substrate) affixed to the inside surfaces of the duct for electrically heating the walls. The gold surface was outermost, i.e. exposed to the air stream. The Intrex was supplied in a roll approximately 1m wide. The electrical conductivity of the sheet was mapped prior to cutting in order to select regions where the conductivity was most nearly uniform. Variations of up to ±5% were regarded as acceptable. First-order corrections based upon this resistivity mapping were applied in computing small local departures from a uniform heat transfer rate. Unlike our earlier study, [7] heating was limited to the 180° bend "section" (which actually began from a flange 106mm upstream of the 0° station). On the upper and lower flat end walls of the duct the Intrex sheet was scored into fourteen electrically isolated curved tracks to allow different voltages to be applied thereby compensating for the different path lengths around the bend for each track. (In this way it was possible to achieve essentially a uniform surface heat flux).

Surface wall temperature measurements were made with thermocouples affixed to the back surface of the Intrex sheet at the same stations as the velocity data were taken. At these same stations a thirteen-probe thermocouple rake was traversed across the duct to provide a mapping of the temperature field. Further details are provided in Johnson and Launder [7].

Johnson's [4] estimates of the accuracies of the various measurements are reproduced in Table 1. The same level of uncertainties attach to the present measurements. Since our data have been gathered during winter, however, there is found to be a marked stratification in temperature between the floor and roof of the laboratory and this has led in turn to a variation in the temperature of the inducted air of approximately 0.4°C between the bottom wall and the symmetry plane. Nusselt numbers have been based on the bulk mean temperature but inevitably the circumferential variation of this quantity - particularly in the early stages - will not be precisely the same as if the flow entering the duct had been uniform. Numerical simulations of this test case should therefore take account of this variation in prescribing inlet

Source	Tolerances associated with hot-wire measurements		
	Mean velocity in tangent (single-wire)	Turbulence intensity (single-wire)	Mean velocity in bend (X-wire)
Probe stem	neg	neg	neg
Probe support	neg	neg	neg
Prong interference	-	-	neg
Temperature variation	neg	neg	neg
End conduction	neg	neg	neg
3-D and turbulence	-	-	up to -1.7%
Curve fit	±1.0%	±1.0%	±1.0%
Voltage measurement	±0.5%	±4.0%	±1.0%
Spatial resolution	neg	neg	±0.9%
Misalignment	neg	neg	±0.9%
Tolerance of pitot calibration	±1.4%	±1.4%	±1.4%
Combined tolerance	±1.8%	±4.4%	±2.9%

Source	Tolerances associated with non-isothermal test measurements	
Heat loss	±1.0%	
Power supply	±2.5%	
Reference junction	±1 to ±2%	(lowest near walls)
Heat increase to rake TCs	±1 to ±4%	(lowest near walls)
Local Intrex sensitivity	±4.0%	
Overall variation in heat flux (error in fluid temperature)	±3 to ±5%	(highest near walls)
Combined effect on fluid temperature measurements (items 3, 4 & 6)	±5.0%	
Combined tolerance of dimensionless temperature $\frac{T - T_w}{T_B - T_w}$	±9.0%	
Combined tolerance of Nusselt number	±5.7%	

Table 1

conditions on temperature.

2.2 Presentation and Discussion of Results

Streamwise velocity profiles and turbulence intensities at three diameters upstream of the bend are shown in Figure 3. To facilitate comparisons with the data of Chang et al [2], the profiles are shown as radial traverses at different heights above the lower wall (X = 0 corresponding with the wall surface and X = 1 with the plane of symmetry). The boundary layers are no more than 10mm thick except in the corners and, from the rms intensity profiles, clearly turbulent. The flow is not perfectly symmetric but the variations (due partly to unavoidable asymmetries in the air flow path in the laboratory and to small non-uniformities in the trip wire) are, we believe, small enough not to be of consequence so far as the shear flow development in the bend is concerned.

The development of the velocity field around the bend is shown in Figures 4-7. At 0° the flow pattern (Figure 4) shows little change from that at the initial station save that the boundary layers have become somewhat thicker, while the effects of the streamwise pressure gradient induced by the bend (favourable on the inside, adverse on the outside) are just visible. By 45° major effects of the imposed streamline curvature are evident in Figure 5. A large inviscid core remains ($0.5 \leqslant X \leqslant 1$) in which turbulence levels are low, while the mean streamwise velocity increases from the outside to the inside of the bend as required for an irrotational vortex. As expected, the boundary-layer-induced secondary flow from the outside to the inside of the bend is confined to the vicinity of the flat lower wall: only for X = 0.125 is V negative. Over the remainder of the duct there is a return flow from the inside to the outside with a peak magnitude of about 15% of W_b.

The flow pattern at 90° shown in Figure 6 provided a major surprise, for the peaks and troughs in streamwise velocity near the inner wall found earlier in the case of fully-developed flow were also present in this case even though the inlet boundary-

layer thickness was here only 10% of the hydraulic diameter. Due to the continual transfer of slow moving fluid to the inside of the bend, the boundary-layer thickness on the convex surface in the range $0.5 \leqslant X \leqslant 1.0$ extends to the centre of the duct. Judging from the low levels of turbulence intensity, there remains a patch of inviscid flow beyond this. Turbulence intensities are generally higher near the convex than the concave wall, a result which must again arise from the continual accumulation of near-wall - and, thus, highly turbulent - fluid on the inside of the bend. The effects of curvature, which would tend to augment turbulence levels near the concave wall and suppress them near the convex surface, are evidently secondary.

An interesting feature near the concave wall is the great variability in the boundary-layer thickness - as evidenced by the w and v intensity profiles near this outer boundary. The layer is thickest and the turbulence levels greatest on the mid-plane; at X = 0.75 fluctuation levels are noticeably lower, while at X = 0.5 there is only a small perturbation above the background level at entry to the duct. This variation seems to suggest the existence of a Gortler-type vortex extending roughly halfway from the symmetry plane to the lower wall. Such a structure would not be surprising since counter-rotating vortices of this type are an endemic feature of "two-dimensional" boundary layers developing on concave walls. The only reason that their presence in this square sectioned duct is in question is that the strong overall secondary circulation could possibly prevent such smaller-scale vortices from forming. At 135° the secondary peak in streamwise velocity is still clearly evident, Figure 7, but at X = 1.0 and 0.75 less pronounced due to the fact that here the near-wall fluid is moving considerably faster. By this position virtually all the fluid is rotational.

The raw temperature profiles at four stations in the bend, shown in Figure 8, exhibit a peak in temperature at the 90° and 135° positions corresponding with the troughs in the velocity profiles, though the latter are more marked. These temperature traverses have been consolidated to produce the isotherm contours in Figure 9. The contours reveal, in some respects

more clearly than the velocity profiles, the nature of the secondary circulation. The coolest fluid is displaced towards the lower inside corner, while there is a marked "eruption" of fluid away from the convex wall near the centre plane. There are, however, no signs of there being an "island" of hotter fluid detached from the wall as there was for fully-developed entry conditions (Johnson and Launder [7]). Evidently the secondary flow created in the two cases is significantly different at 90° despite the superficial similarity of the velocity profiles.

The development of the Nusselt number distribution around the perimeter of the duct is presented in Figure 10. The results are shown as if the two curved surfaces were folded down flat to be co-linear with the bottom wall. Because heating begins only at the start of the bend section (i.e. about 1.4 diameters upstream of the start of curvature), the levels of Nusselt number are significantly above what would be found in fully-developed flow. As would be expected, therefore, by 45° into the bend Nu has fallen, particularly on the convex wall. By 90°, however, the shear layers have grown sufficiently that the associated increase in effects of streamline curvature on turbulence and in secondary flow causes a rise in Nusselt number on the concave wall while depressing further the levels near the mid-point of the convex wall. By 180° the ratio of the Nusselt numbers measured at the mid-points of the concave and convex walls has risen to nearly 2:1. The general distribution at this position is similar to that reported in [7] for the case of nearly fully-developed flow at entry (30 hydraulic diameters of flow development upstream of the bend), the levels of Nu here being lower by about 15% on average. This is an interesting (though not entirely unexpected) outcome because the patterns in the development of Nusselt number up to the 180° position are so strongly different in the two cases.

3. The Computational Programme

The computations of flow in curved, square-cross-section ducts have been made by converting SEDUCT, the UMIST semi-

elliptic solver for circular sectioned ducts, from toroidal to cylindrical polar coordinates. The solution procedure (for toroidal coordinates) has been extensively described by Iacovides [10] and summarized by Iacovides and Launder [6, 11] and Humphrey et al [12]. In this new version we retain all the following features of the original code:

- The usual staggered arrangement of U, V, P nodes with nodal values iterated by way of the SIMPLER algorithm.

- The use of the non-diffusive QUICK scheme [13] for approximating convective transport in the cross-section of the duct.

- An algebraic second-moment turbulence model for representing the turbulent stresses which are solved on a mesh staggered with respect to the velocity nodes. (The standard $k-\varepsilon$ eddy-viscosity model is also retained as an option).

- Stability-enhancing measures applied in iterating the stress field similar to those developed by Huang and Leschziner [14].

- The employment of the Van Driest version of the mixing-length hypothesis in the 4% of the duct hydraulic diameter adjacent to the solid boundary.

One modification in strategy has been reluctantly introduced, however. The PSL scheme [15] which, in the case of a circular sectioned duct, afforded a very economical numerical treatment in the vicinity of the wall (as pressue variations normal to the wall were neglected) had to be abandoned for the case of the square sectioned bend. Pressure variations in the corners due to the strong secondary flow apparently have an essential role to play in causing the flow to change direction. All attempts at using PSL, or several variants thereof, led to divergent behaviour. Accordingly, for the results presented hereunder the pressure field is stored over the entire solution domain.

3.2 Application to 90° Bend with Thin Inlet Boundary Layers

These computations were made with an 25 x 47 x 135 grid and simulated the experiment of Taylor et al [8]. To date, only the k-ε EVM has been employed. Computations began with a uniform flow and proceeded downstream in a straight duct until the mean velocity profile achieved the best fit with the data at the measuring station upstream of the bend. (Perfect agreement could not be achieved for the isotropic eddy-viscosity model is unable to account for the effect of turbulence-driven secondary flows). At this point we synchronized the computational position with that of the experiment.

Figure 11 compares primary and secondary velocities at four stations with the experimental data and the earlier computations of Kreskovsky et al [9]. While the latter predictions are generally in close agreement with the experimental data at 60° and 77.5°, they do not correctly predict the thickening of the streamwise boundary layer near the inside of the bend. The secondary flow prediction there also shows some discrepancies. The present computations employing the k-ε EVM do very much better in this respect. The close agreement is maintained downstream of the bend exit (no results were reported at that position by Kreskovsky et al). Indeed, the agreement between the computed and measured development is probably within the uncertainty of the experimental data.

3.3 Fully-Developed Flow Passed Around a 180° Bend

The simulation in this case is of the experiment by Chang, Humphrey and Modavi [1] of flow in a U-bend with a mean bend radius:hydraulic diameter ratio of 3.375:1. Flow entered the bend after development in a straight inlet tangent of 31 hydraulic diameters. Johnson [4] subsequently performed an experiment at the same Reynolds number in an identically proportioned bend but with an inlet of 72 hydraulic diameters. His results suggest that from 90° onwards the flow-field data were essentially the same in the two experiments.

field. The velocity vectors in the plane of the cross-section are shown in Figure 13. As one proceeds from the 45° to 135° stations, the single elliptic secondary vortex becomes grossly distorted and finally breaks down into four separate vortices.

More extensive comparisons of the computed behaviour with the experimental data (including detailed comparisons with the thermal field) will be made in a paper now in preparation.

4. Conclusions and Proposals for Further Work

This short research programme has contributed to both experimental and computational aspects of the problem of flow in curved ducts. Concerning the experiments, it has provided a further detailed set of velocity- and thermal-field data of flow in square sectioned U-bends. Like the earlier studies on fully-developed flow passing through an identically proportioned bend, the present measurements show that between 45° and 90° a major upheaval occurs in the boundary-layer development near the convex wall with a marked near-wall velocity peak appearing and, beyond this, a patch of slow moving, highly turbulent fluid.

It had been our expectation in planning this experiment that, with thin inlet boundary layers, a simpler flow pattern would emerge than for the case of fully developed conditions at bend entry. The simplification was sought because experience had shown that the fully-developed case seemed well beyond what current computational schemes could predict; a somewhat simpler intermediate case was thus seen as helpful in pointing the way forward. The present experimental results suggest, however, that the case of thin boundary layers presents a challenge to the predictor that is scarcely less severe. Clearly, the 180° bend provides a far more searching test than the 90° bend where, for the case of thin inlet boundary layers, the very simple turbulence model employed by Kreskovsky et al [9] achieved a moderately satisfactory prediction of the flow development recorded by Taylor et al [8].

Although there has not been scope within the present grant

Choi [17] has earlier reported k-ε EVM predictions with a different code from the present one but constructed on the same principles. His computations did not agree well with experiment, though they were an improvement on the earlier computations of Chang [2] and Johnson [4] who employed wall functions instead of a low-Reynolds-number turbulence model to span the near-wall sublayer.

In view of these prior calculations, the present study has focused on applying the algebraic second-moment closure, ASM. The computations were made with fully-developed entry conditions and although this did not precisely correspond to the experiment it seems, from what is noted above, that these differences should not significantly affect the computations at 90° and beyond. The grid employed was 25 x 47 x 100 which required approximately 500 passes to reduce the absolute mass residuals, summed over the whole domain, to below 4% (i.e. less than 0.04% imbalance per plane).

The development through the bend of the streamwise velocity along different radial lines is shown in Figure 12. At 45° into the bend there is little difference between Choi's EVM results and the present ASM computations. Both are in reasonable agreement with experiment if one accepts that at this station, for reasons unknown, the measured bulk velocity (obtained by orifice meter) is about 6% too high.

By 90° a rather different picture has emerged. This is the first station at which the experimental streamwise velocity profiles showed strong secondary maxima near the inside of the bend - a feature almost entirely missed by the EVM computations. The ASM computations in contrast <u>do</u> exhibit double maxima. While agreement with experiment is by no means perfect, the degree of accord is evidently greater than for the EVM computations. At 135° a similar picture emerges, only here there is even closer agreement between the ASM computations and experiment.

It is of interest to note the computed secondary flow pattern that gives rise to this complex streamwise velocity

to generate computations of the new data, simulations of earlier experiments have helped to clarify the capabilities of present turbulence transport models. Firstly, for the flow of Taylor et al noted above, essentially complete agreement with experiment has been achieved, even with the standard k-ε eddy-viscosity model. For the case of the 180° bend flow of Chang et al, our ASM computations go a considerable way towards removing the large disagreements found by Choi when using the k-ε EVM.

The above results suggest that there are two follow-up sets of computations that ought to be made as soon as possible. Firstly, in view of the spectacularly good agreement for the 90° bend data of Taylor et al, the 180° bend case of Chang et al needs to be re-computed employing the k-ε EVM to ascertain whether the behaviour predicted by this model really is as bad as other studies have indicated. Professor Choi employed PSL in making his fine-grid computations, a practice we were forced to abandon due to abiding failure of the iteration scheme to converge. It thus needs to be checked whether the suppression of pressure variations in the corner that occurs with PSL could have been the reason that Choi's computations showed only a marginal improvement over the earlier wall-function results.

The second set of computations that urgently need to be made are simulations of the new experimental data here presented. This is a situation that is closer to the case of a centrifugal impeller than any of the other "fundamental" data sets for a square sectioned bend: the boundary layers are thin and the bend turning angle is greater than 90°. The success of EVM and ASM computations in describing this flow will give a clear indication of whether current generation turbulence models are adequate for predicting flow in turbomachinery blade passages.

Acknowledgements

The experimental programme relied heavily on the dedicated and skilful technician support provided by Mr. Dennis Cooper. Thanks are also due to Mr. D.C. Jackson for advice and assistance in many aspects of the experiments. Mr. H. Iacovides' ASM

computations of flow in a 180° bend were supported by Rolls-Royce PLC as part of a study of flow in rotating ducts. Partial support for Mr. P. Loizou's computations of flow in a 90° bend has been provided by the SERC under research grant GR/D65367. Finally, our thanks go to Mrs. L.J. Ball for typing and compiling this report.

References

1. Chang, S.M., Humphrey, J.A.C. and Modavi, Physico-Chemical Hydrodynamics 4, 243, 1983.

2. Chang, S.M. PhD Thesis, University of California-Berkeley, Mechanical Engineering Department, 1983.

3. Chang, S.M., Humphrey, J.A.C., Johnson, R.W. and Launder, B.E. Proc. 4th Symp. on Turbulent Shear Flows, Karlsruhe, 1983.

4. Johnson, R.W. PhD Thesis, Faculty of Engineering, University of Manchester, 1984.

5. Launder, B.E. and Iacovides, H. "Computation of Flow and Heat Transfer in Flow Around a 180° Bend," Final Report on USONR Power Program Contract N00014-83-G-0021, UMIST Mech. Eng. Dept. Report TFD/85/5(R), 1985.

6. Iacovides, H. and Launder, B.E. Proc. 4th Int. Conf. on Numerical Methods in Laminar and Turbulent Flow, Vol. 2, 1023-1045, Pineridge Press, Swansea, 1985.

7. Johnson, R.W. and Launder, B.E. Int. J. Heat and Fluid Flow 6, 171, 1985.

8. Taylor, A.M.F., Whitelaw, J.H. and Yianneskis, M. ASME J. Fluids Eng. 104, 350, 1982.

9. Kreskovsky, J.P., Briley, W.R. and McDonald, H. "Prediction of Laminar and Turbulent Primary and Secondary Flows in Strongly Curved Ducts," NASA Report CR-3388, 1981.

10. Iacovides, H. PhD Thesis, Faculty of Technology, University of Manchester, 1986.

11. Iacovides, H. and Launder, B.E. 1st UK National Heat Transfer Conf., IChemE Series 86, 2, 1097, 1984.

12. Humphrey, J.A.C., Iacovides, H. and Launder, B.E. J. Fluid Mech, 154, 357, 1985.

13. Leonard, B.P. Comp. Meth. in Appl. Mech. and Eng., 19, 59, 1979.

14. Huang, P.G. and Leschziner, M.A. Proc. 5th Symp. on Turbulent Shear Flows, 20.7, Cornell, 1985.

15. Iacovides, H. and Launder, B.E. J. Fluids Eng. 106, 245, 1984.

16. Choi, Y.D. Personal communication.

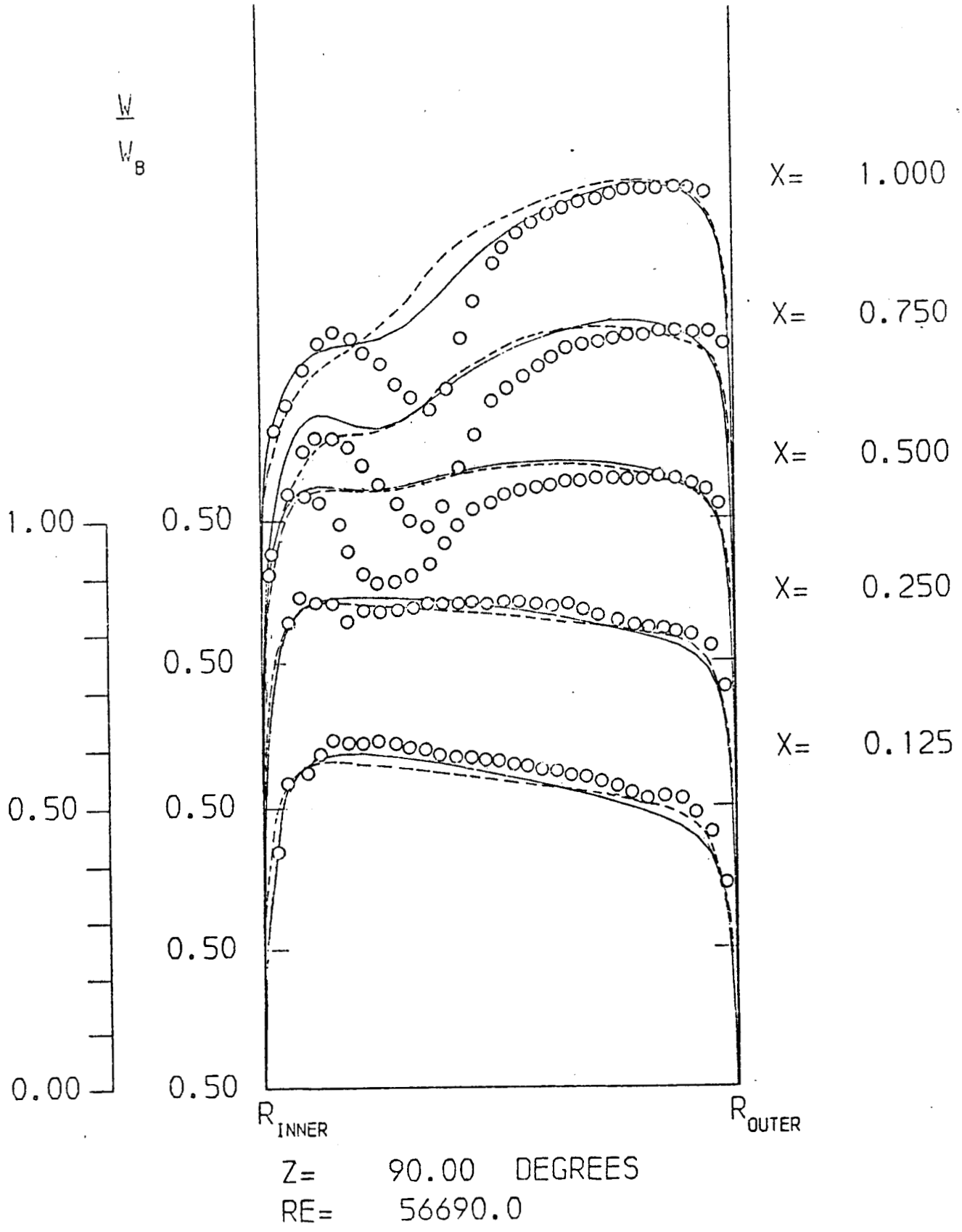

Fig. 1 Streamwise velocity profiles at 90° plane of 180° bend

Symbols : measured velocity profiles [1]
Broken line : computations with wall functions [4]
Solid line : Choi's computations with refined grid and low-Reynolds-number near-wall model

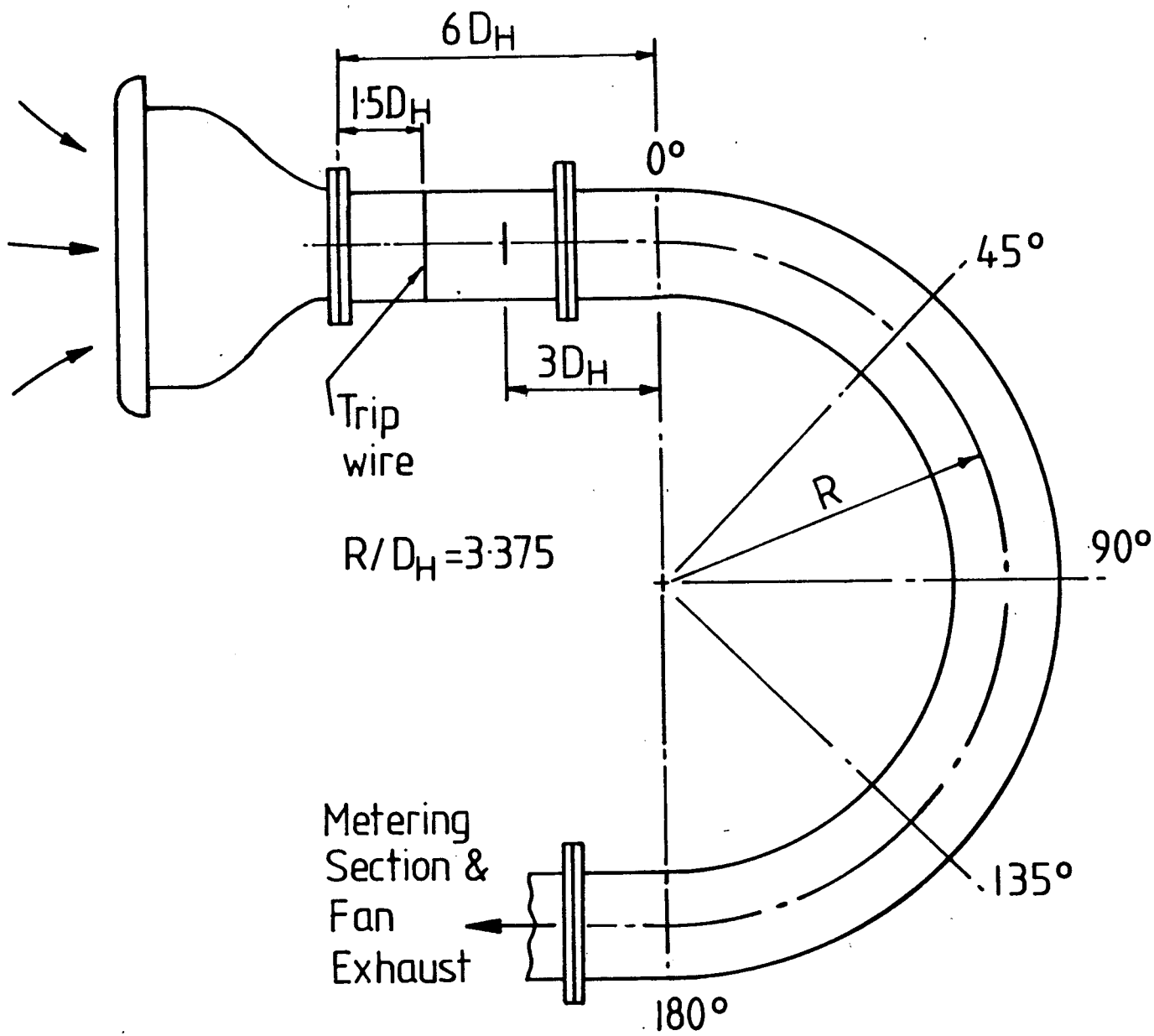

Fig. 2 Schematic diagram of apparatus

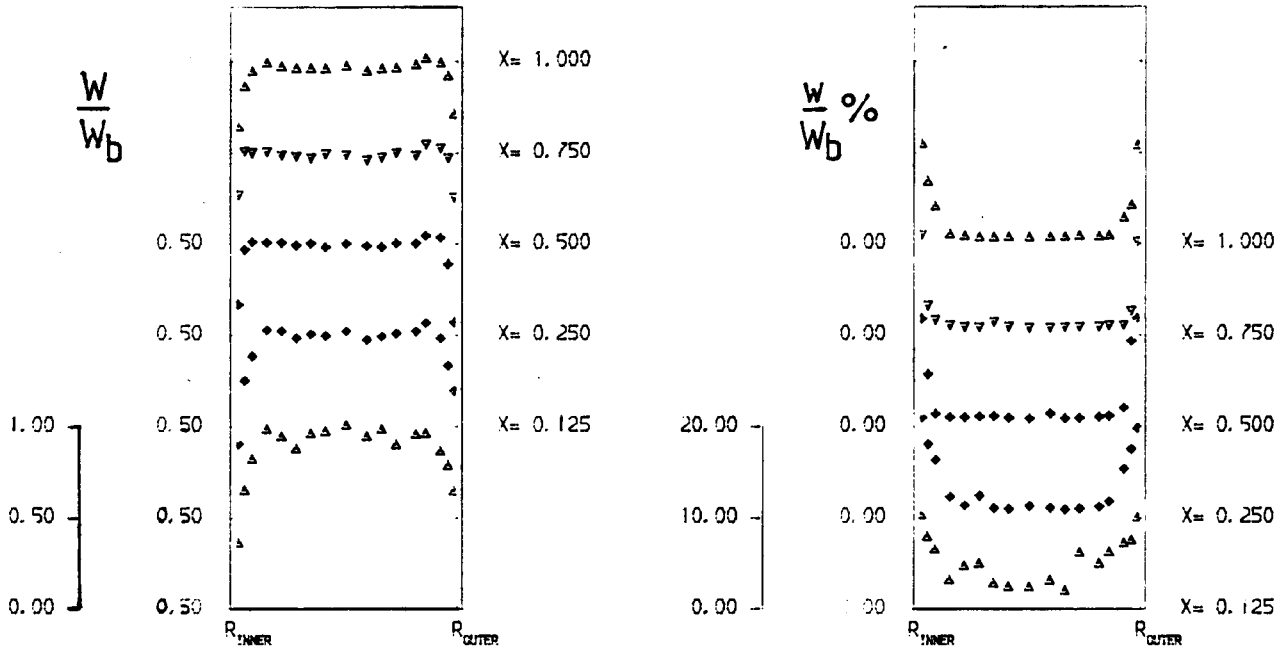

Fig. 3 Streamwise velocity and turbulence intensity at 3 D_H upstream of bend

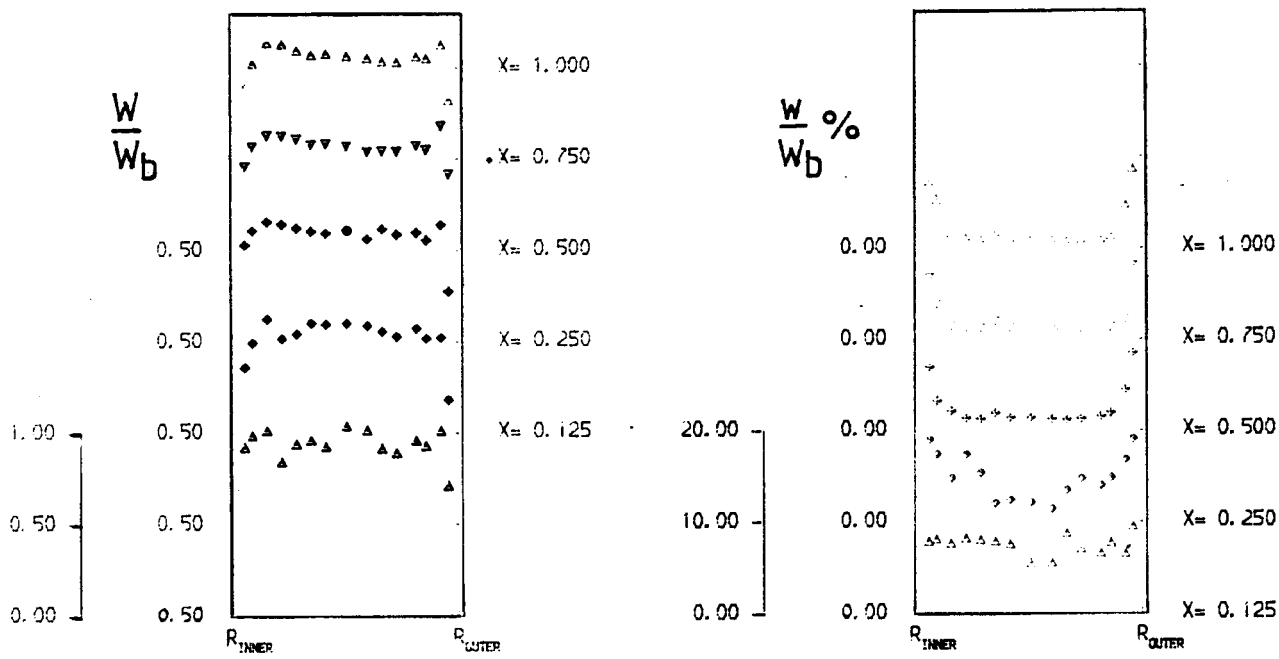

Fig. 4 Mean and turbulent velocity profiles at entry to bend

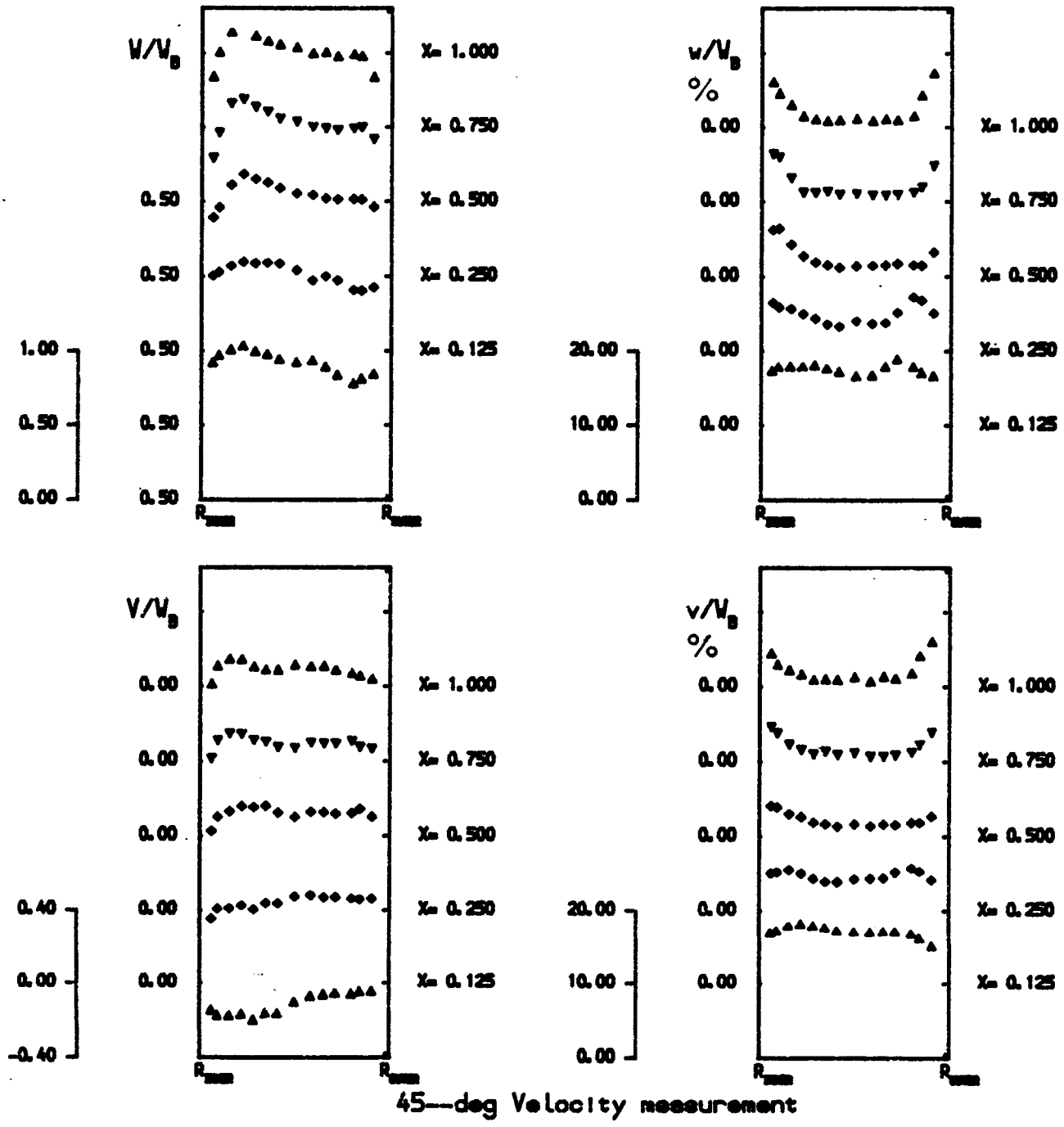

Fig. 5 Axial and radial mean and turbulent velocity profiles at 45° station

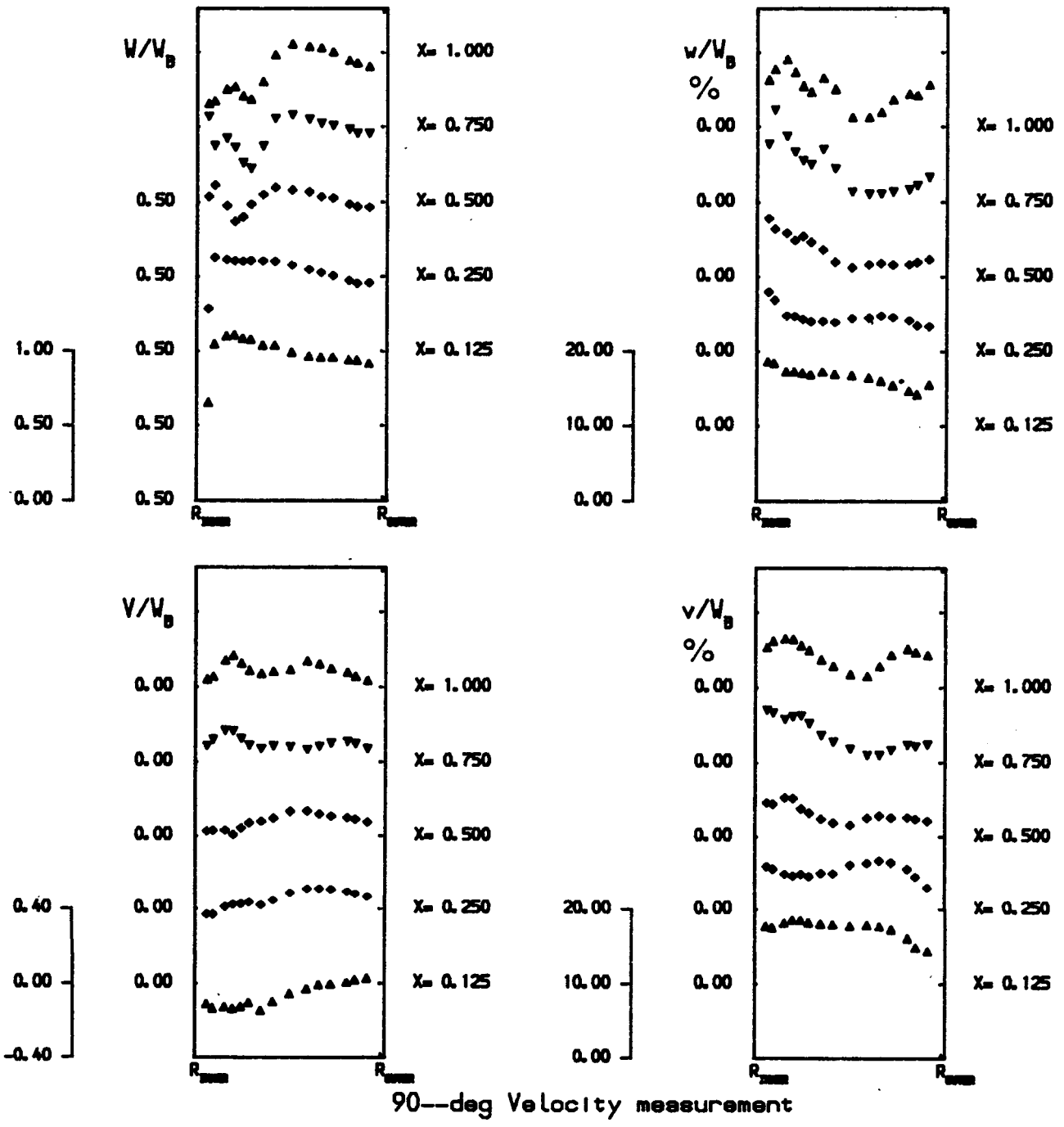

Fig. 6 Axial and radial mean and turbulent velocity profiles at 90° station

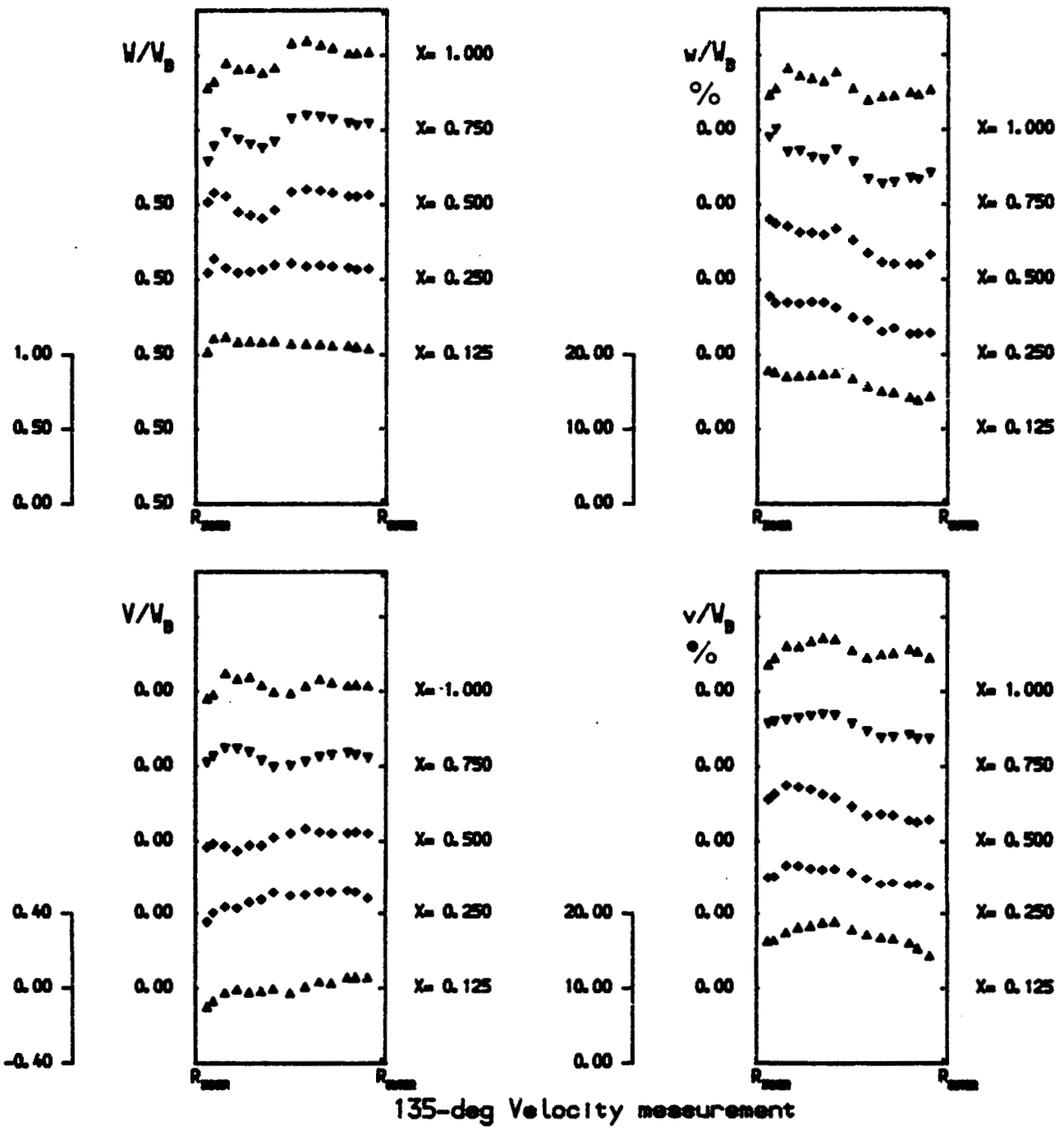

Fig. 7 Axial and radial mean and turbulent velocity profiles at 135° station

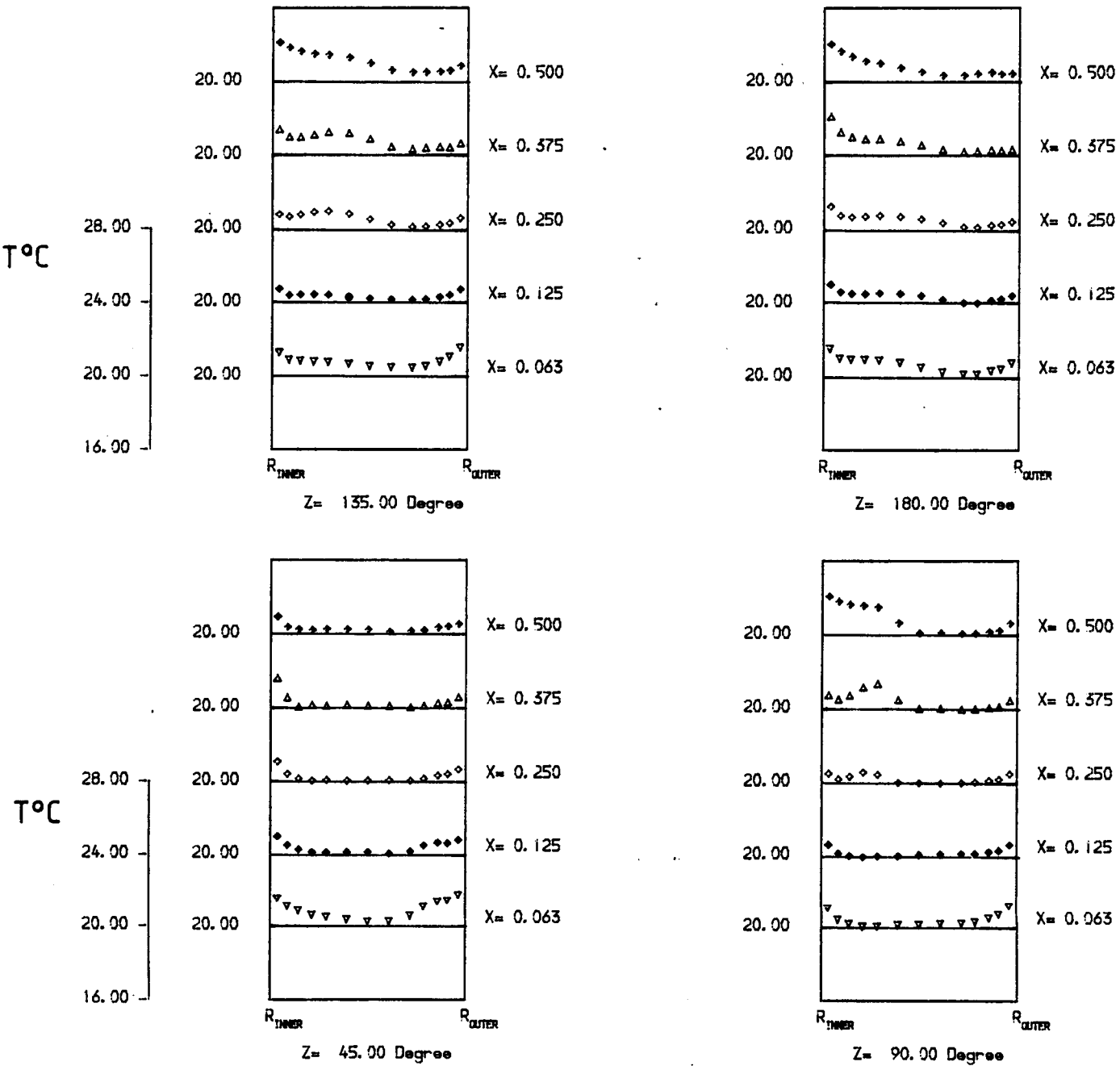

Fig. 8 Mean temperature at four stations in bend

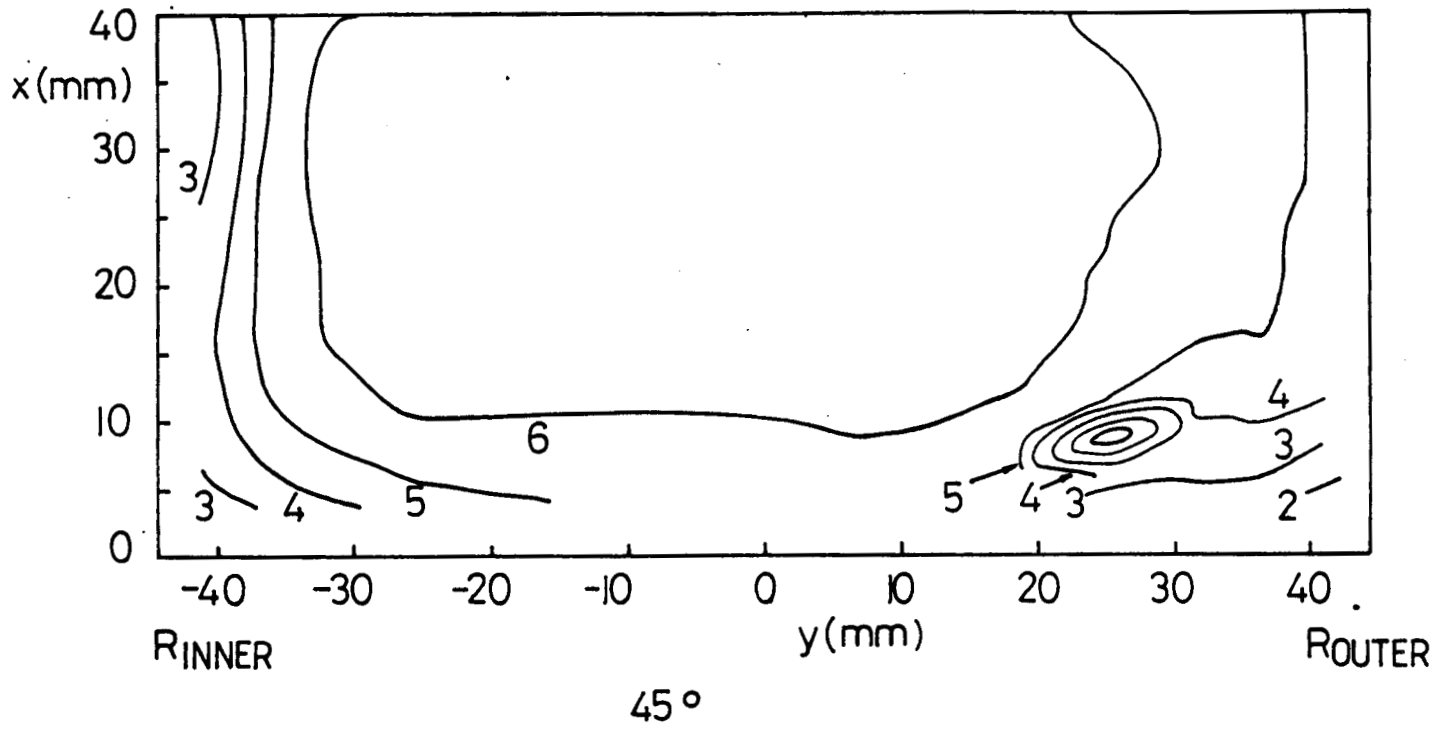

Fig. 9a

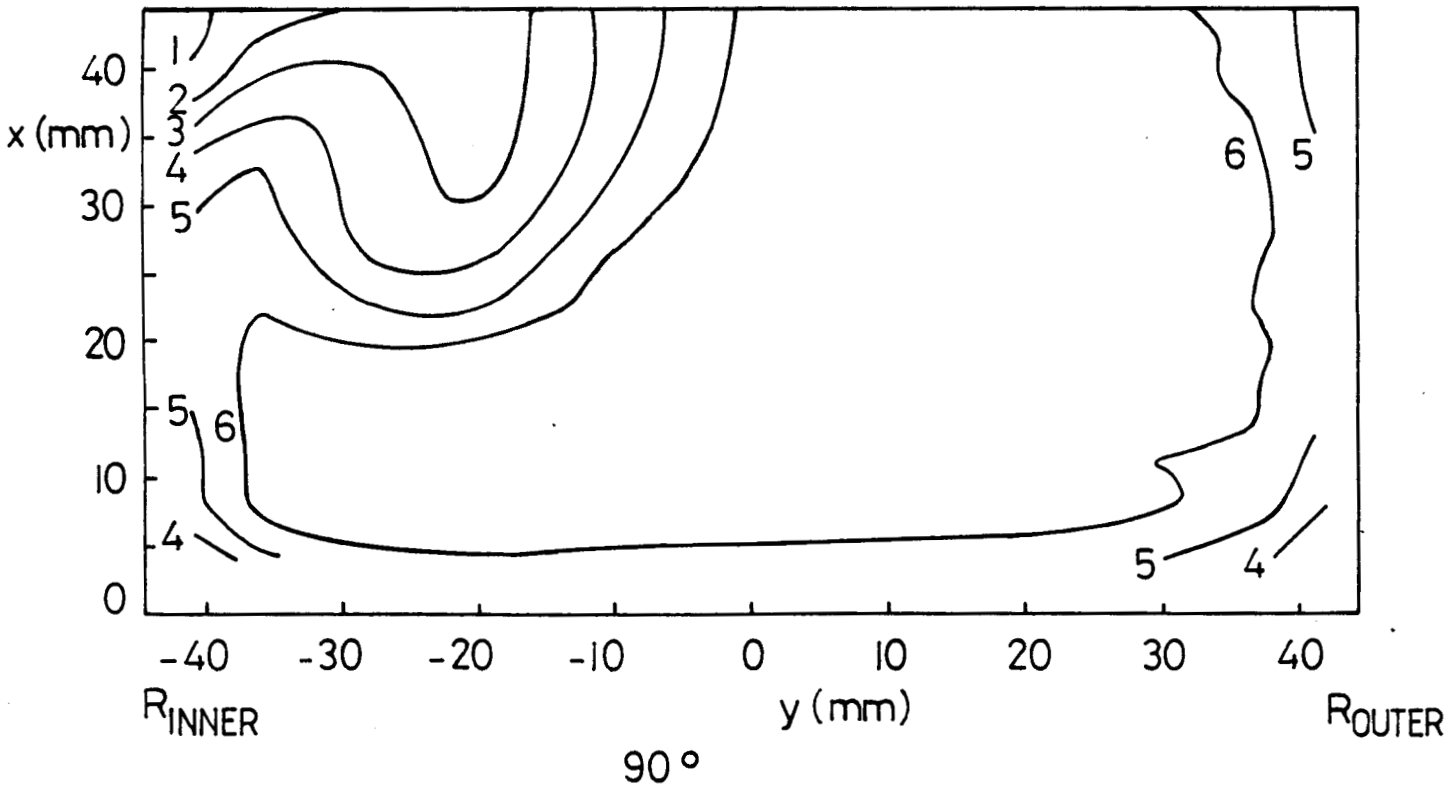

Fig. 9 Isotherm patterns in the bend

Contour numbers denote the following temperatures:
1 = 22.5°C ; 2 = 22°C ; 3 = 21.5°C ; 4 = 21°C ; 5 = 20.5°C ; 6 = 20°C

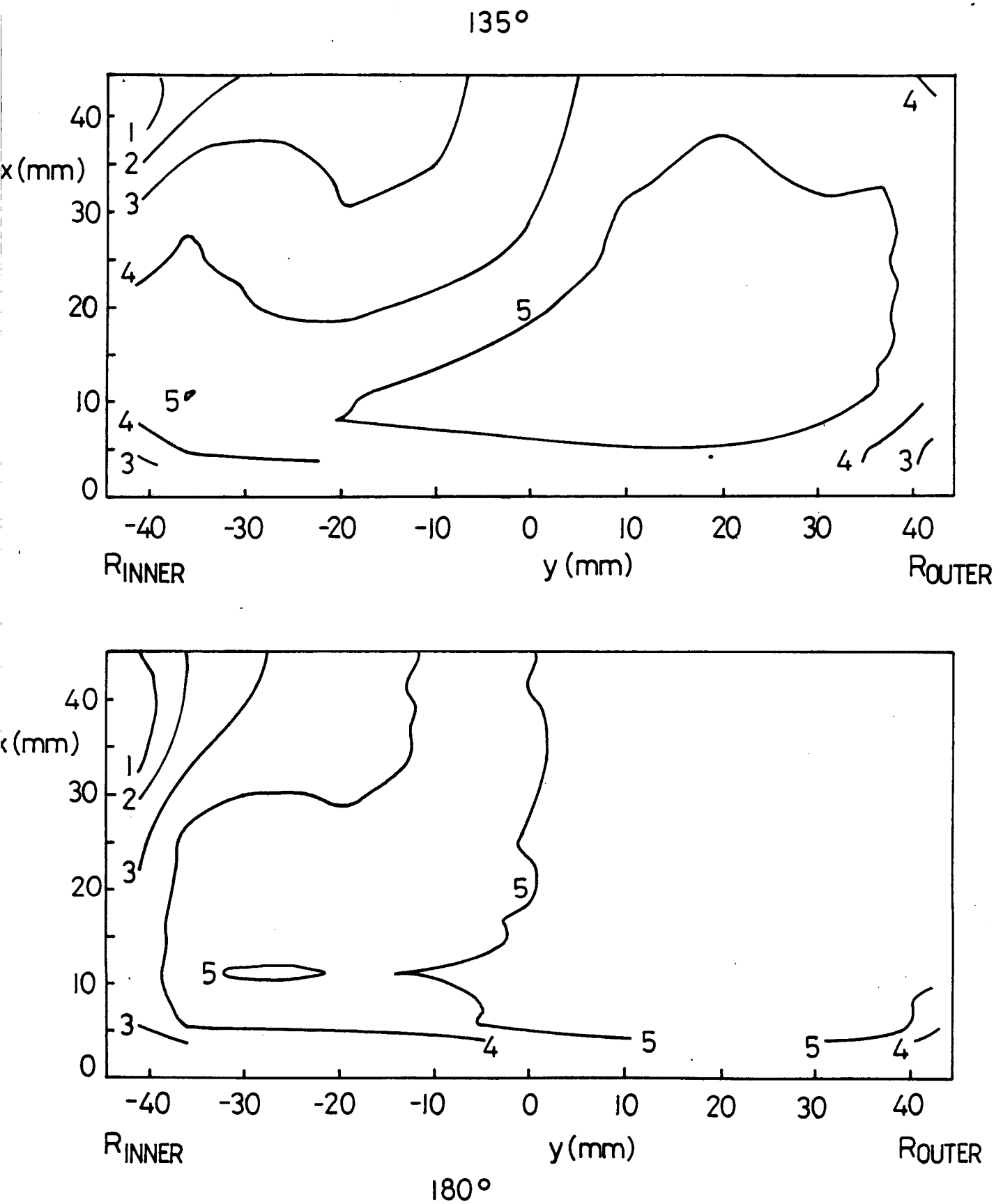
135°
x (mm)
40
30
20
10
0
1
2
3
4
5
-40
-30
-20
-10
0
10
20
30
40
RINNER
y (mm)
ROUTER
x (mm)
y (mm)
180°

Fig. 9b

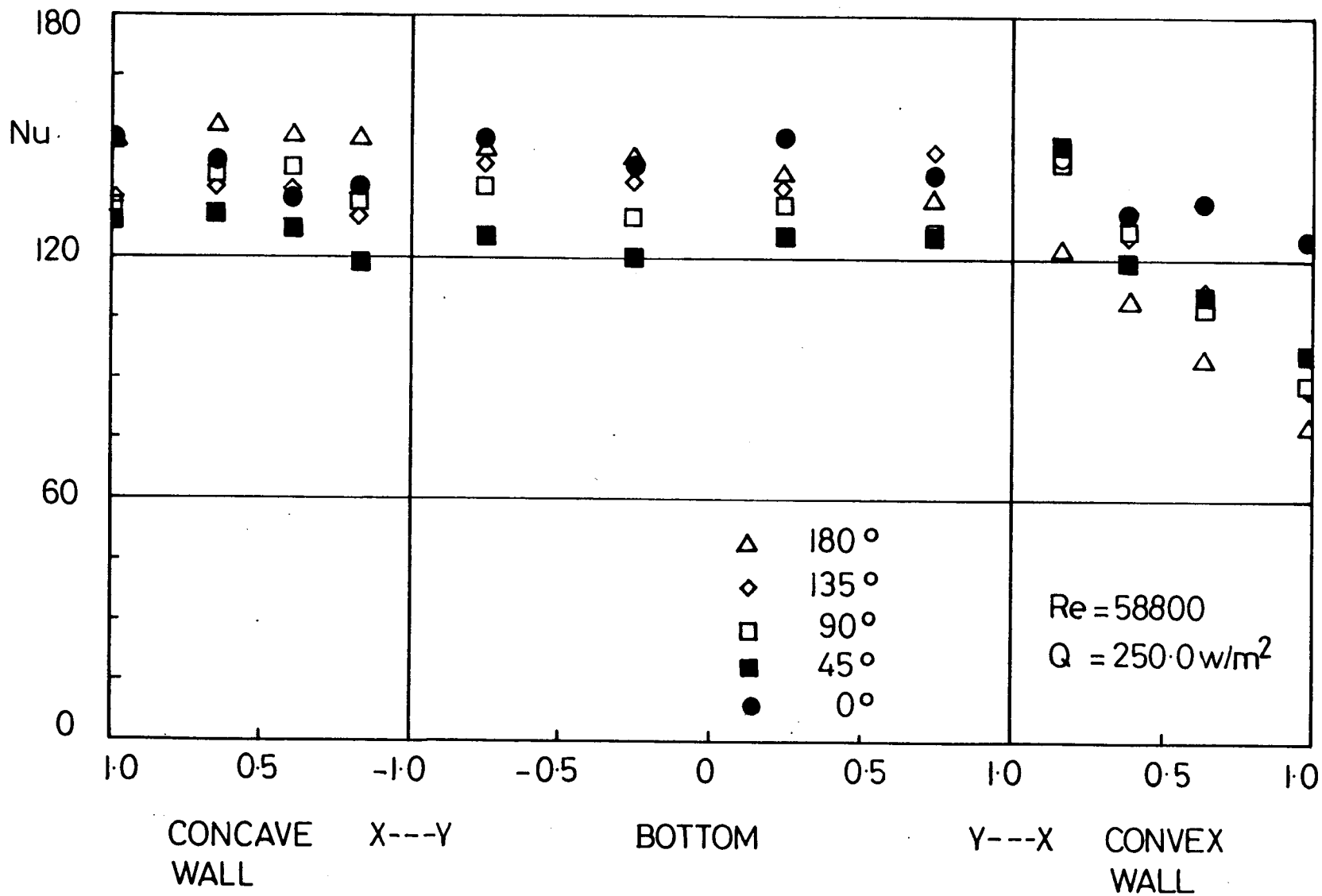

Fig. 10 Development of local Nusselt number around bend

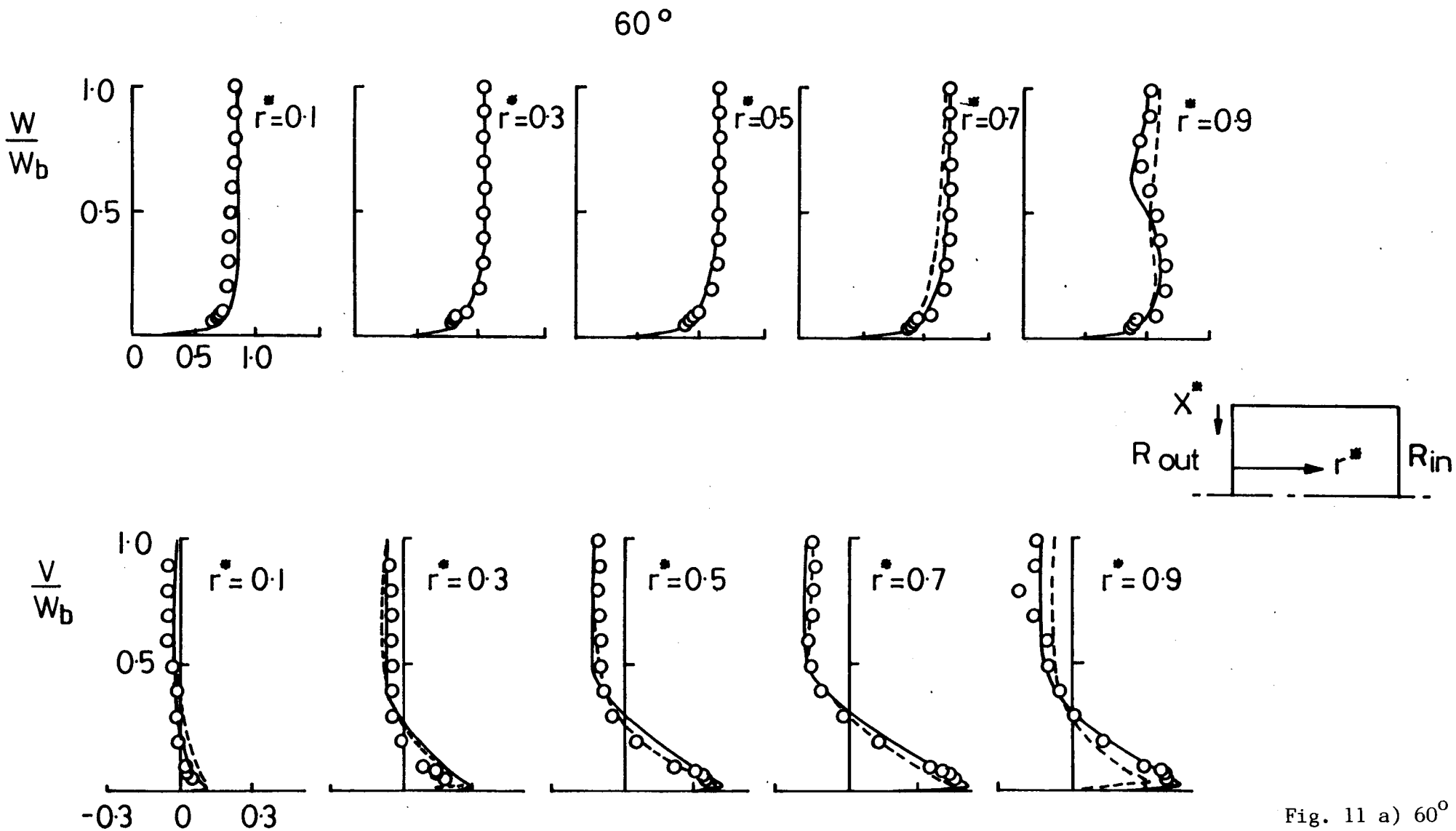

Fig. 11 a) 60°

Fig. 11 Primary and secondary mean velocity profiles at four stations

o o o o Experiments Taylor et al [8]
——— Present computations
- - - - - - Kreskovsky et al [9] computations

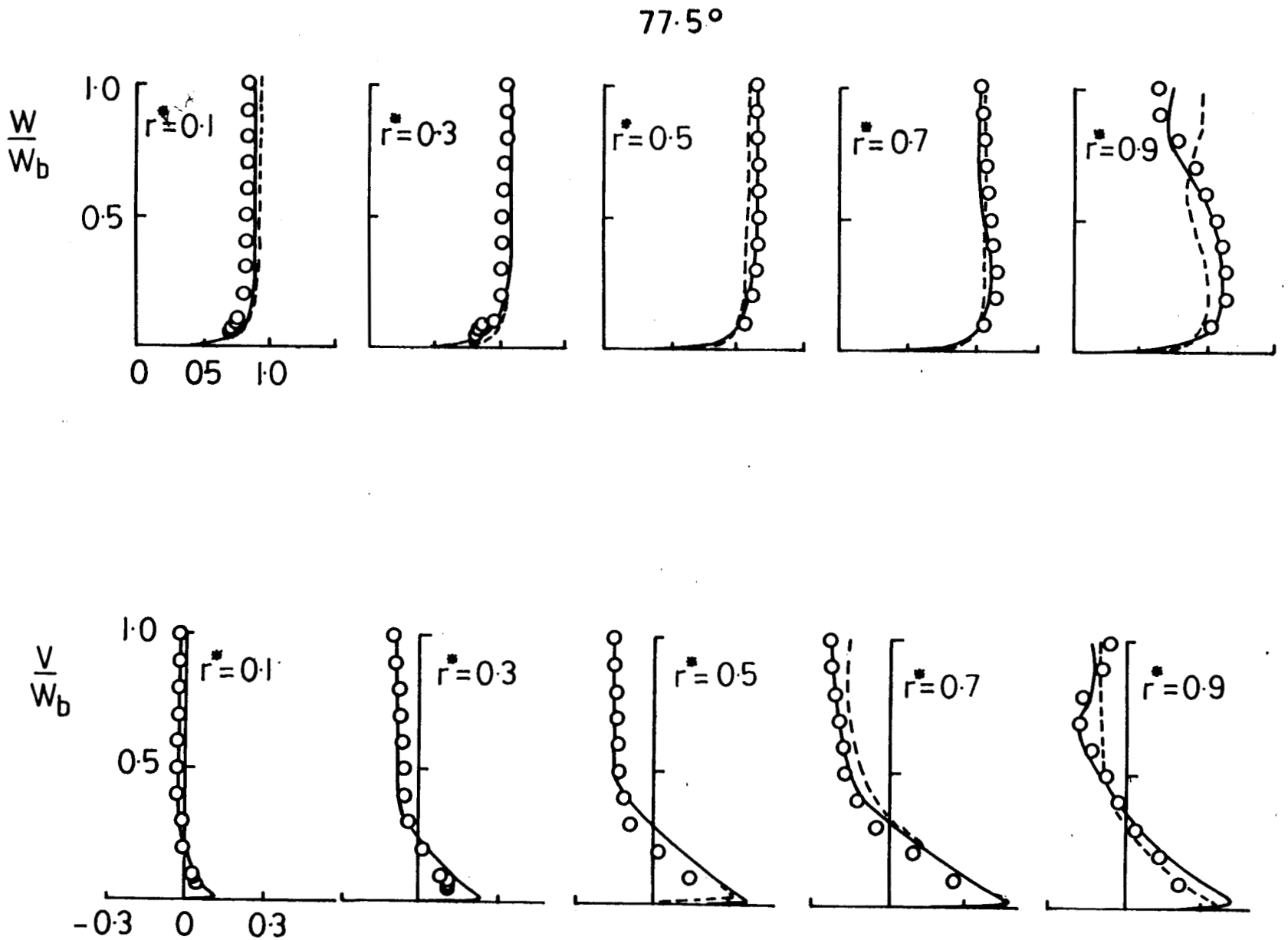
77·5°
W/Wb
1·0
0·5
0
05
1·0
r*=0·1
r*=0·3
r*=0·5
r*=0·7
r*=0·9
V/Wb
1·0
0·5
-0·3
0
0·3
r*=0·1
r*=0·3
r*=0·5
r*=0·7
r*=0·9

Fig. 11 b) 77.5°

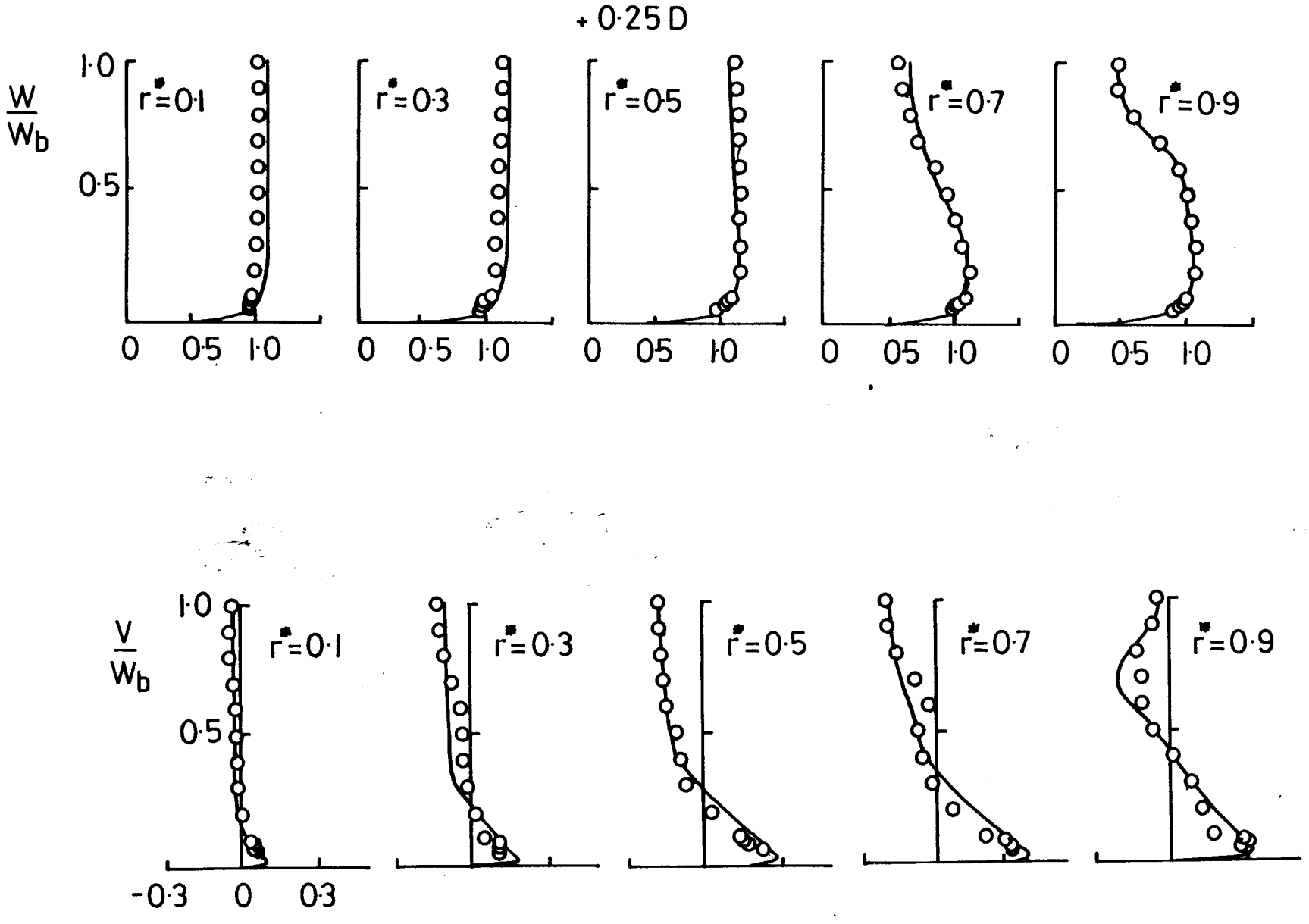

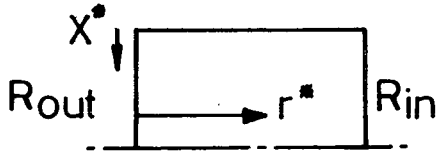

Fig. 11 c) 0.25 D_H downstream

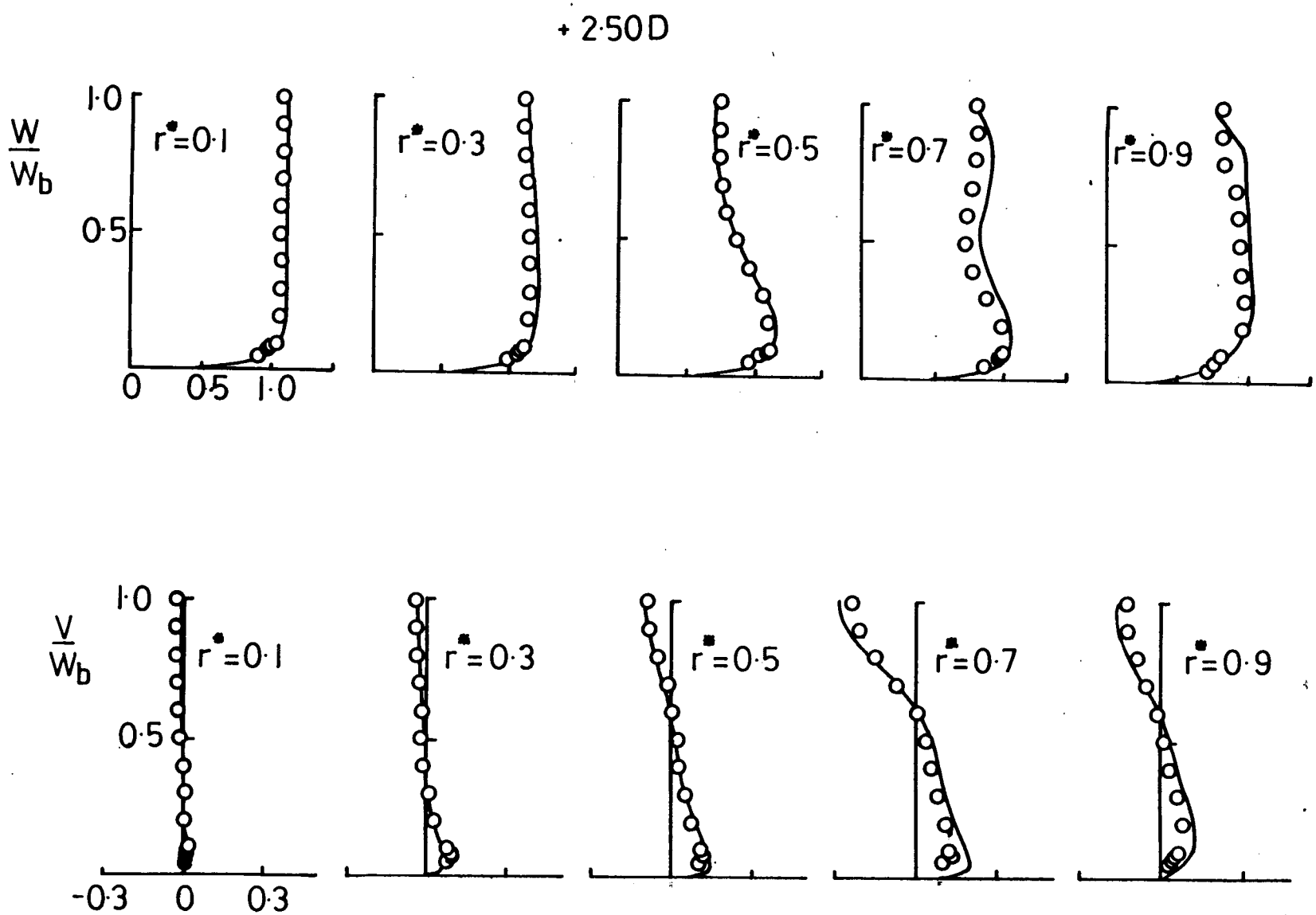

Fig. 11 d) 2.5 D_H downstream

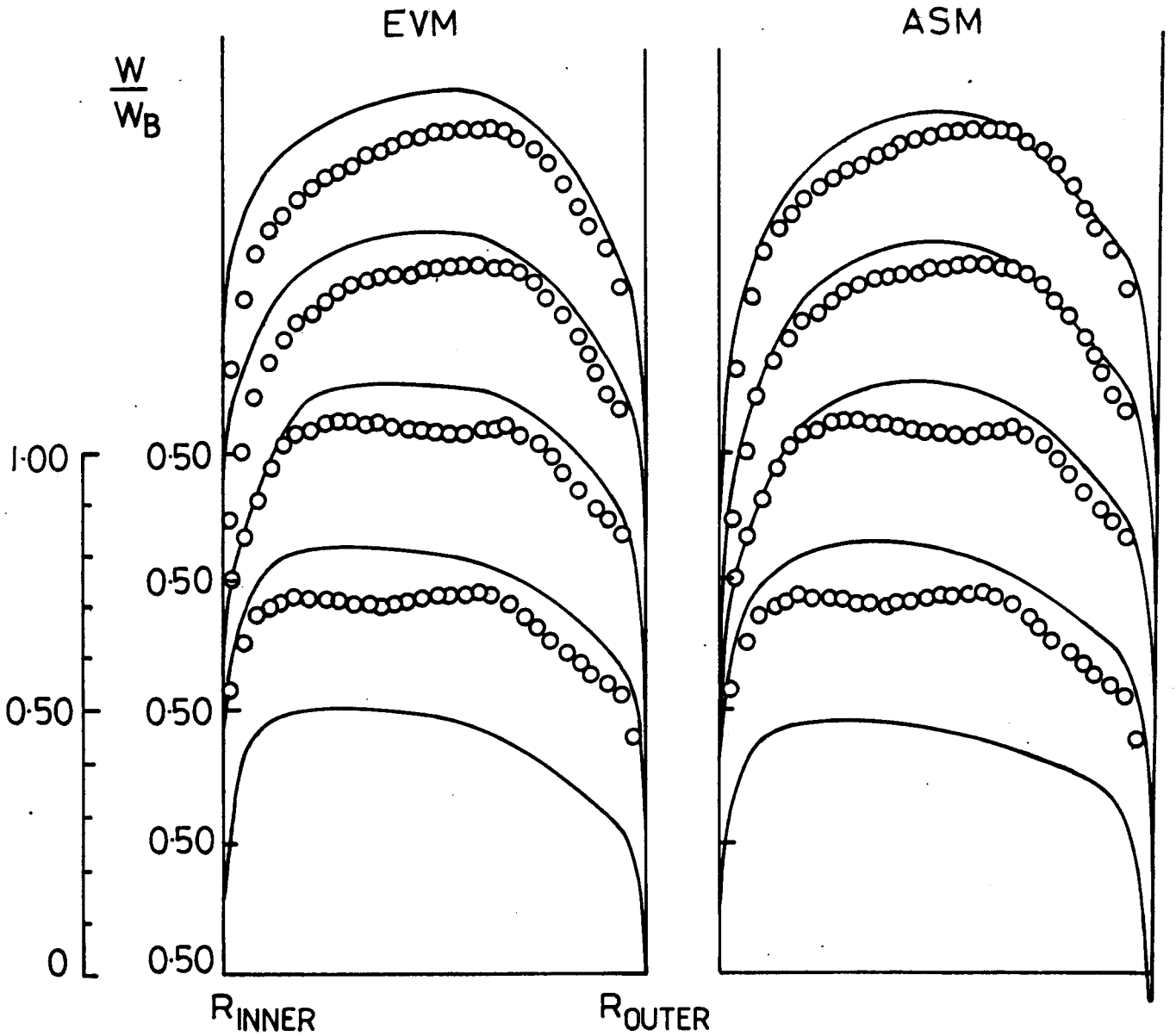

Fig. 12 a) 45°

Fig. 12 Computed streamwise velocity profiles in turbulent flow around 180° bend

Symbols: Experiments Chang et al [1]

Lines : Computations

Left-hand figures show k-ε results by Choi [5]
Right-hand figures show ASM computations from present study

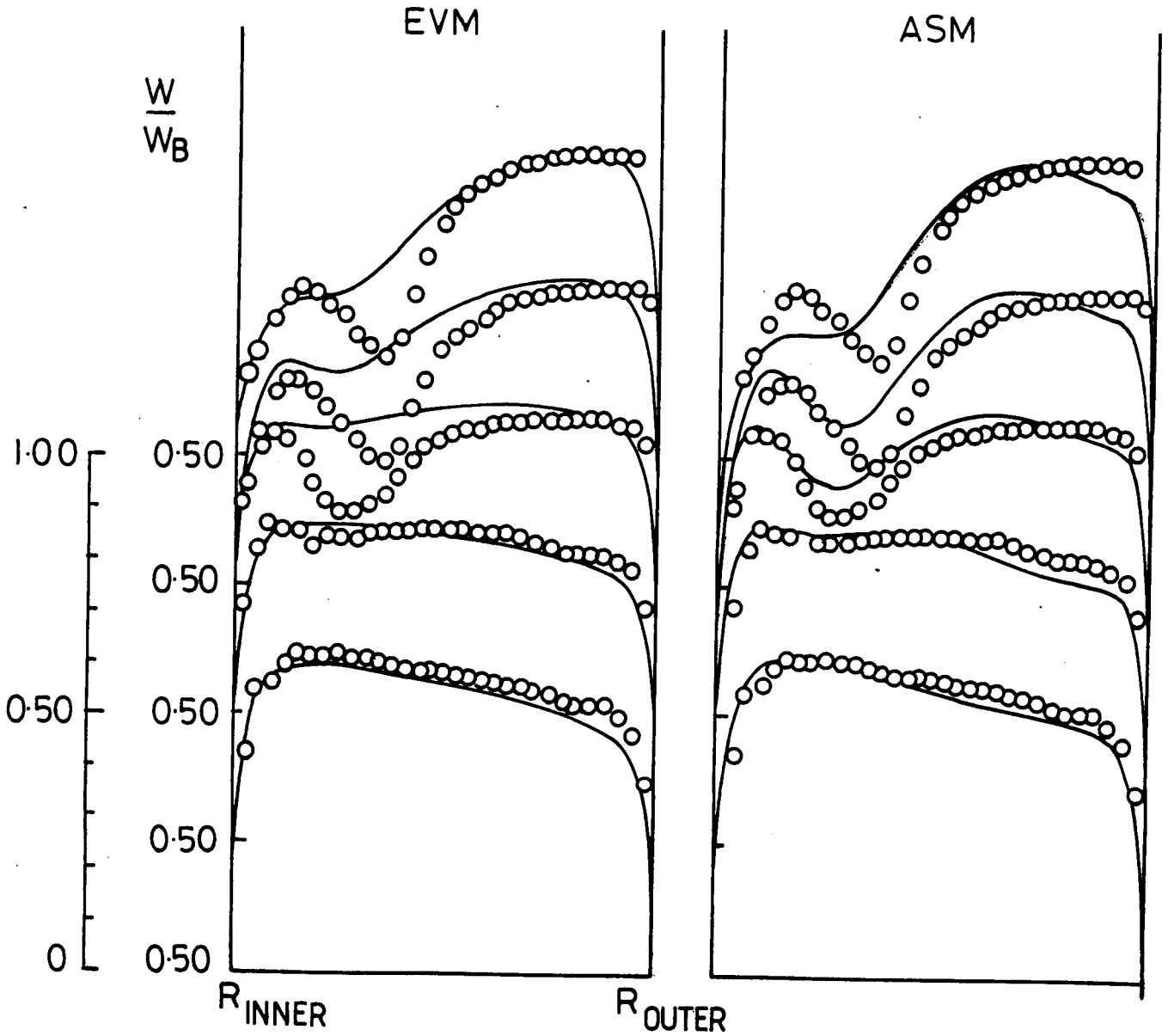

Fig. 12 b) 90°

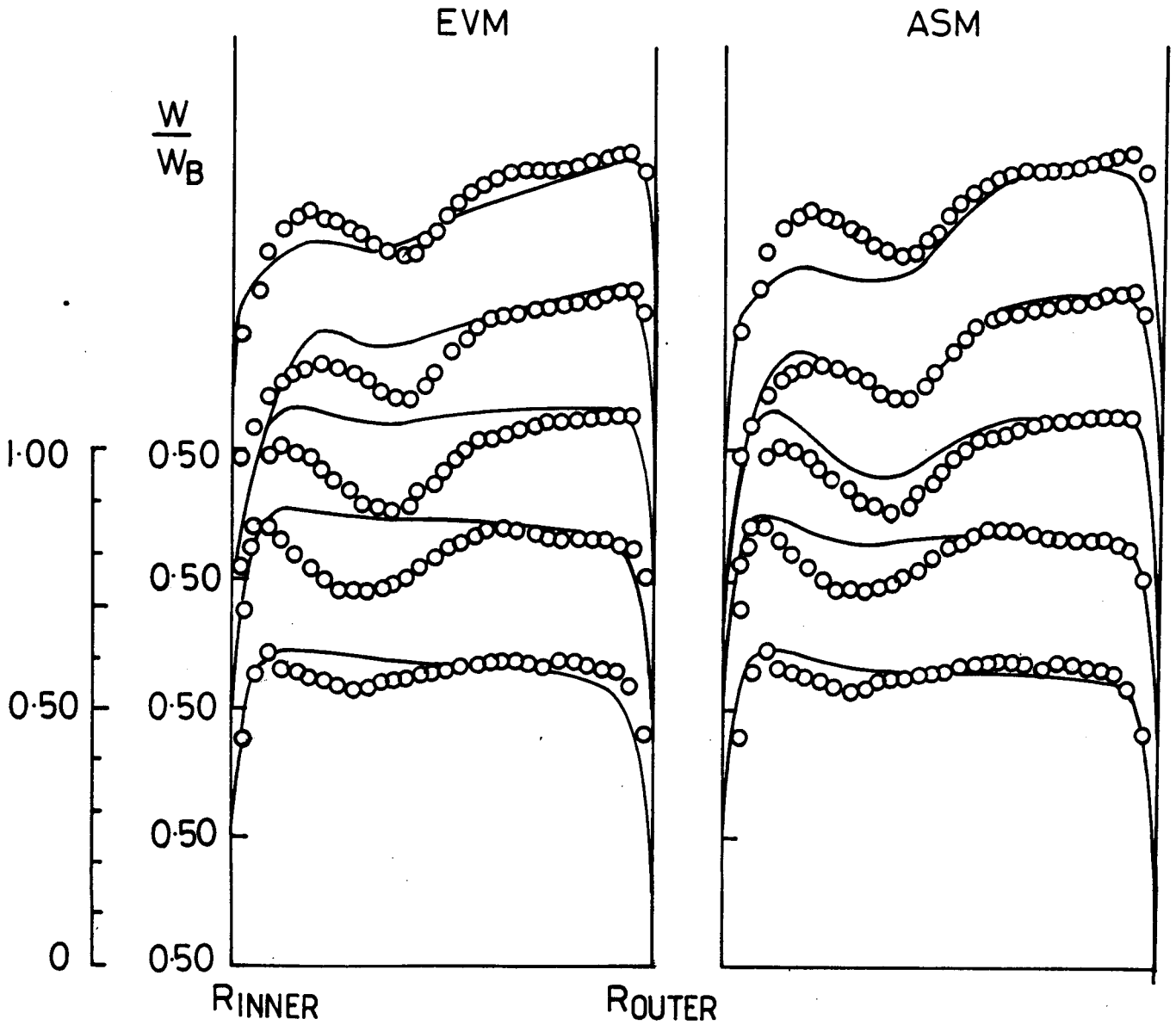

Fig. 12 c) 135°

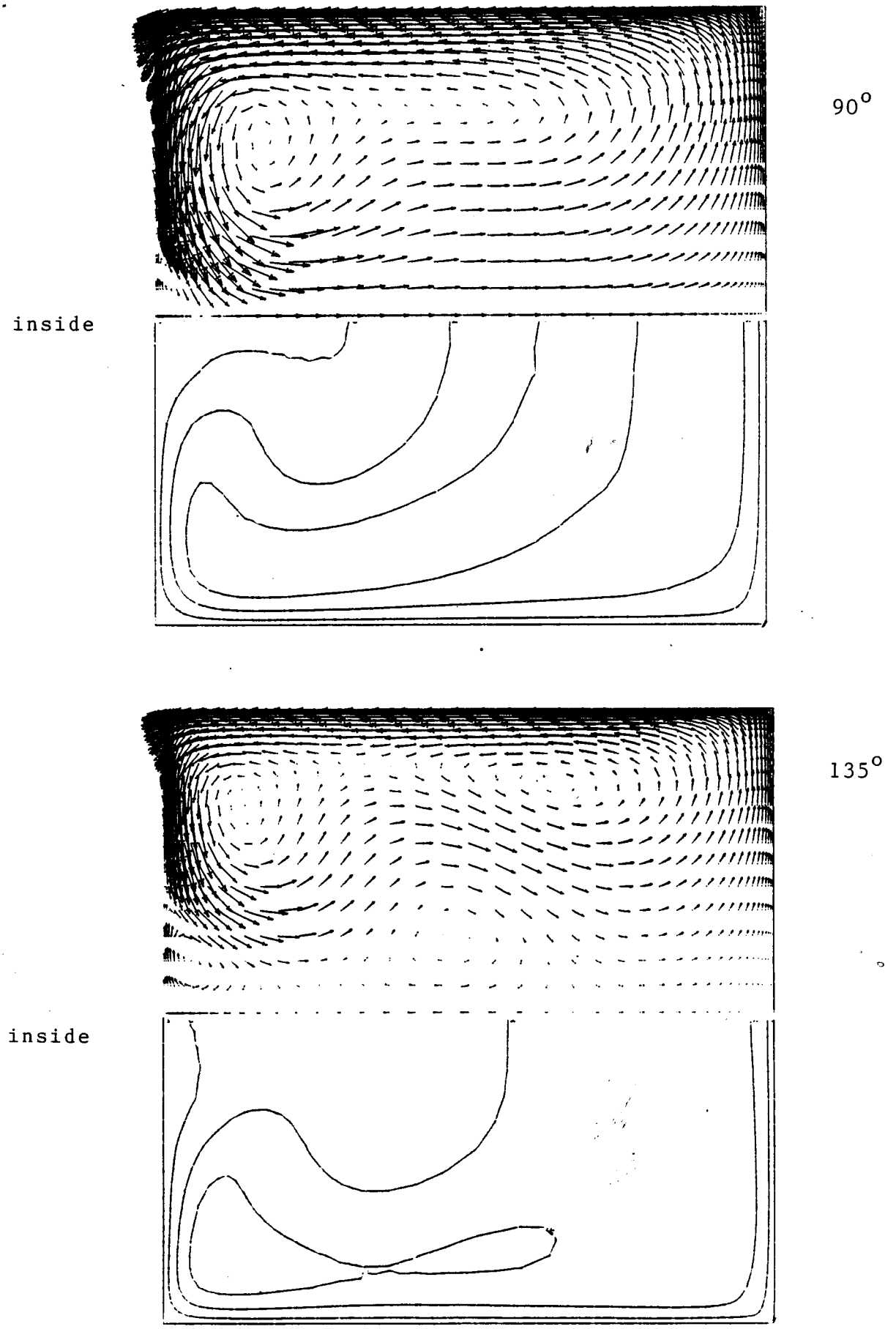

Fig. 13 Computed secondary flow velocity vectors/Axial velocity contours
ASM turbulence model